metals

MDPI

Article

Thermodynamics Analysis and Pilot Study of Reusing Medium and High Alloy Steel Scrap Using Induction Melting and Electroslag Remelting Process

Liushun Wu, Kunlong Liu, Haiqing Mei, Guangda Bao, Yun Zhou * and Haichuan Wang

School of Metallurgical Engineering, Anhui University of Technology, Maanshan 243032, China; wuliushun@ahut.edu.cn (L.W.); ahutlkl@ahut.edu.cn (K.L.); mhq18856218721@ahut.edu.cn (H.M.); bgd98@ahut.edu.cn (G.B.); which@ahut.edu.cn (H.W.)

* Correspondence: zhouahut@aliyun.com; Tel.: +86-139-5558-5501

Abstract: The annual cumulative quantity of high and medium alloy steel scrap has exceeded 10 million tons. Using the traditional smelting process involving electric arc refining in a smelting furnace for these scraps causes high percentages of alloy losses, which decreases the value of the alloy steel scrap and poses environmental threats. Existing studies have rarely focused on separate smelting of the scrap and oxidation behaviors of the alloying elements. Therefore, this study proposes an induction melting and electroslag remelting scheme to process the scrap. Based on this scheme, the effects of the temperature, oxygen content, and element contents on the recovery percentages of the alloying elements were investigated using pilot experiment and thermodynamic analysis. The experimental results showed that the alloying elements (tungsten, chromium, nickel, molybdenum, and vanadium) exhibited recovery percentages of 97.36%, 94.62%, 97.63%, 95.09%, and 89.49%, respectively; furthermore, the impurity content did not increase during smelting. The thermodynamic analysis indicated that an increase in carbon content improved the oxidation resistance of the alloying elements except for nickel, whereas the increases in the contents of oxygen and alloying elements increase their oxidation. Steam partial pressure and air suction dramatically increase the concentrations of nitrogen, hydrogen and oxygen. This scheme is an alternative for smelting medium and high alloy steel scrap, and the thermodynamic analysis provides a theoretical understanding of the oxidation behaviors of the alloying elements in the steel scrap and the control of impurity.

Keywords: alloyed steel scrap recycling; alloying element oxidation; thermodynamics analysis; induction smelting; electroslag remelting

check for updates

Citation: Wu, L.; Liu, K.; Mei, H.; Bao, G.; Zhou, Y.; Wang, H. Thermodynamics Analysis and Pilot Study of Reusing Medium and High Alloy Steel Scrap Using Induction Melting and Electroslag Remelting Process. *Metals* **2022**, *12*, 944. https://doi.org/10.3390/met12060944

Academic Editors: Jianhua Liu, Yang He and José Spinelli

Received: 2 April 2022
Accepted: 24 May 2022
Published: 30 May 2022

Publisher's Note: MDPI stays neutral with regard to jurisdictional claims in published maps and institutional affiliations.

Copyright: © 2022 by the authors. Licensee MDPI, Basel, Switzerland. This article is an open access article distributed under the terms and conditions of the Creative Commons Attribution (CC BY) license (https://creativecommons.org/licenses/by/4.0/).

1. Introduction

The global cumulative quantity of steel scrap reached 460 million tons in 2020, including production waste [1], processing residues [2], and end-of-life products [3,4]. Therein, the quantity of medium (5–10% of the total alloy content) and high (greater than 10% of the total alloy content) alloy steel scrap, accounting for approximately 3% of the total steel scrap, amounted to more than 10 million tons. Considering that the production of medium and high alloy steel consumes several ferroalloys, whose production is an energy-intensive and a mineral-resource-intensive process, the recovery of the steel scrap may reduce the consumption of energy and natural resources. Therefore, extensive studies on the efficient utilization of steel scrap that will provide economic and environmental benefits are necessary [5–8].

Currently, ordinary steel scrap is usually smelted in an electric arc furnace [9–12], and alloy steel scrap is usually treated as ordinary steel scrap [13]. A small part of medium alloy steel scrap is used as a supplementary alloy for producing alloy steel using the conventional smelting process [14,15] (electric arc furnace smelting with ladle refining and Ruhrstahl–Heraeus (RH) refining). During smelting, electric arc zone reaches an excessive

temperature of over 3000 °C, which accelerates the oxidation of reactive metals in terms of kinetics. Thereby, to reduce the losses of alloys, alloying is performed in the late stage of smelting. Obviously, the above method cannot be implemented to medium and high alloy steel scrap smelting. Thereby, electric arc furnace smelting results in a relatively low recovery percentage of the alloying elements [16] and decreasing the value of the alloy steel scrap. Furthermore, hazardous substances (oxides of the alloying elements) form dust and slag, posing environmental threats. Hence, it is necessary to determine more efficient processes.

Compared to an electric arc furnace, a medium-frequency induction furnace is more suitable for diversified small-lot production of medium and high alloy steels. Moreover, using a medium-frequency induction furnace for melting steel scrap is advantageous as it offers direct input of heat into the metal that ensures rapid heating, controlled bath movement that guarantees uniform temperature, high thermal efficiency, and easy implementation [17]. A previous study indicates that, in the alloying process, adding a molten alloy (melted in the induction furnace) provided a much higher yield than that obtained when adding a solid alloy [18]. This study aimed to produce an alloy steel using ferroalloys. In addition, medium-frequency induction was widely used for casting [19,20] and alloy preparation [21]. Notably, literature on the usage of a medium-frequency induction furnace in the recycling of alloy steel scrap is extremely limited. Moreover, a general induction furnace is known to present the practical difficulty of docking during the ladle and RH refining processes. Electroslag remelting processes purify steel effectively [22], such as dehydrogenation [23], desulfuration [24,25], deoxygenation [26] and declusion [27], and it is gradually applied to produce high quality medium and high alloy steel [28]. From a metallurgical perspective, a method that combines medium-frequency induction melting and electroslag remelting of the ingots is worth exploring.

H13 grade steel, also known as martensitic die steel (containing 1.1–1.75% Mo, 0.8–1.2% V, 4.75–5.50% Cr, 0.8–1.2 % Si, 0.2–0.5% Mn, 0.32–0.45 %C, $\leq$ 0.03% S, and $\leq$ 0.03% P), is an example of a medium alloy steel, which is widely used in various applications, such as die casting molds, hot extrusion molds, high-speed fine forging molds, and forging press molds, owing to its excellent strength and plasticity [29,30]. Correspondingly, the amount of H13 grade steel scrap has increased rapidly in the past decades [31,32].

Hence, this study, taking H13 grade steel scrap as an example, aimed to investigate the oxidation behaviors of the alloying elements in medium and high alloy steel scraps during medium-frequency induction furnace smelting. In addition, considering the contents of the impurities severely affect the performances of the steel, for example, nitrogen deteriorating the weldability [33,34] and plasticity of steel [35,36], hydrogen inducing cracking [37–39], inclusion decreasing the plasticity and toughness of the steel [40], the variation in the contents of S, P, N, H, and O in the ingots were evaluated. This study provides an alternative method for the efficient recycling of medium and high alloy steel scraps.

2. Materials and Methods

H13 grade steel scrap was dried in an oven at a temperature of 393 K for 3–4 h. In addition, approximately 3000 kg of dried steel scrap was placed in a medium-frequency induction furnace; the furnace had a capacity of 3000 kg, diameter of 1 m, height of 1.5 m, and power of 2 MW with an operating frequency of 1 kHz. Approximately 100–150 kg of the mixture of premelted refining slag and metallic aluminum (for inhibiting alloy oxidation, accounting for about 10% of the slag) was used to cover the steel scrap. Metallic aluminum helps alleviate the oxidation of alloy. Next, the scrap was melted by heating for 70–80 min, melt temperature approximated 1650 °C (infrared system of temperature measurement) and then, held for 5–10 min. Meanwhile, 99.999% pure Ar was injected into the molten steel from the bottom of the furnace at a flow rate of 10–15 L/min for Ar stirring. The contents of the alloying elements in the samples were analyzed using a quartz tube with a diameter of 5 mm for sucking the liquid steel. Moreover, supplemental alloying was performed by adding master alloys (i.e., a base metal) in the following sequence, according

to the compositions of the targeted H13 grade steel and its variants: ferrotungsten (FeW70), ferrochrome (FeCr69C0.5), nickel plate, ferromolybdenum (FeMo60), and ferrovanadium (FeV50). Finally, the molten steel was cast into ingots with a diameter and length of 250 and 1200 mm, respectively. Each ingot from the medium-frequency induction furnace was treated in an electroslag remelting furnace to produce an electroslag ingot. In the remelting process, the mass ratio of slag (30% Al_2O_3 + 70% CaF_2) to steel was 4:100. The schematic of the process is shown in Figure 1.

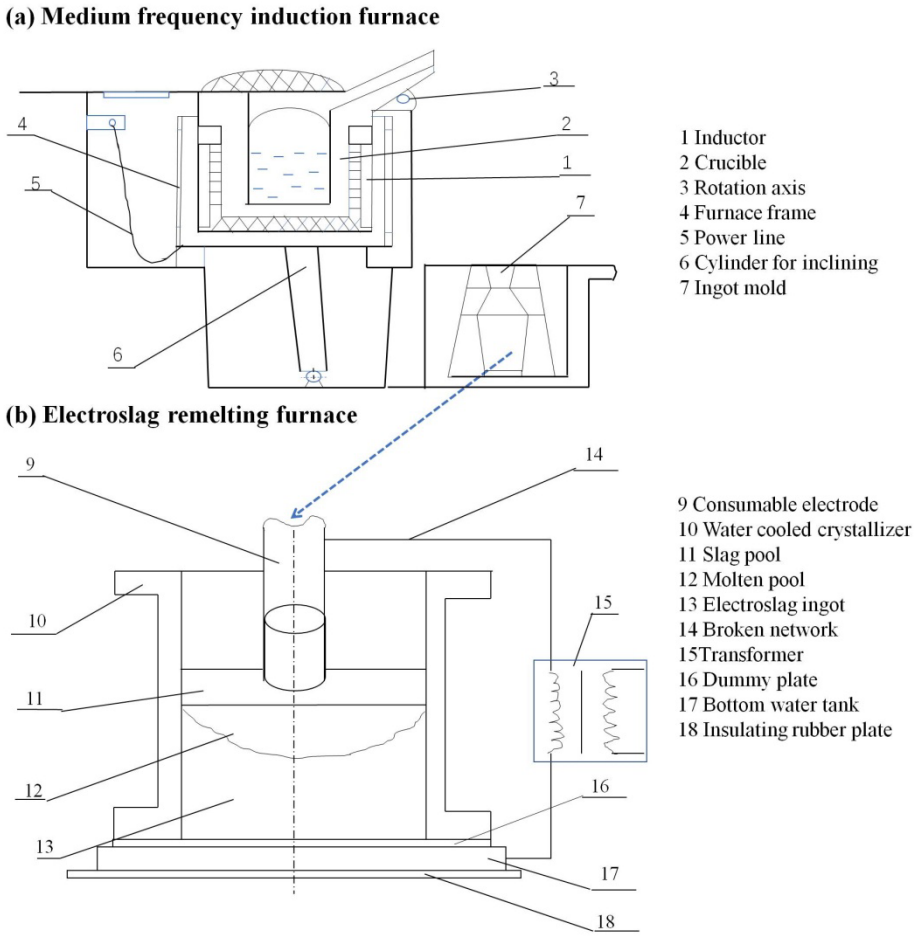


Figure 1. Schematics of medium-frequency induction furnace and electroslag remelting furnace.

The samples obtained from the induction furnace and steel scrap were cut and ground, and their chemical compositions were determined immediately using a spark direct reading spectrometer (FOUNDRY-MASTER Smart). Moreover, analyses were conducted via scanning electron microscopy (SEM; JSM-6510) and energy dispersive spectroscopy (EDS; INCA Feature X-Max 20) to verify spinel formation in the samples from induction furnace. Chemical compositions of the slag used in the induction furnace were determined using X-ray fluorescence spectrometer. Tables 1 and 2 listed the chemical compositions of steel scrap and the slag.

Table 1. Chemical composition range of H13 grade steel scrap used (wt%).

W	Mo	Ni	V	Cr		Mn
0.07–0.09	1.10–1.20	0.16–0.20	0.80–0.90	5.00–5.30		0.31–0.40
C	**Si**	**S**	**P**	**O**	**N**	**H**
0.35–0.45	0.86–0.98	0.0040–0.0080	0.016–0.020	0.0018–0.0025	0.0053–0.0056	0.0015–0.0018

Table 2. Chemical composition range of the premelted refining slag (wt%).

CaO	Al_2O_3	SiO_2	MgO	S
40–48	40–46	<4	<6	<0.1

A block from each ingot in the induction furnace was processed into a crumb powder using a driller, which was then dissolved in 100 mL of HNO_3 with a concentration of 38.3 mass%. The amounts of impurities, such as P and S, in the obtained solution were determined using inductively coupled plasma atomic emission spectrometry (ICPS-7510 PLUS). Five samples were obtained from each electroslag ingot. One sample, which was used for the H content determination, was cut into several pieces with a weight of 1 g; the other two samples, which were used for O and N content determination, were smoothened to a roughness of 6.13–12.5 μm, and then, cut into several pieces with a weight of 1 g. All pieces were cleaned using CCl_4 in an ultrasonic cleaning tank (UC-10, Biocomma; Shenzhen, China). Furthermore, the amounts of H, N, and O were all determined using an oxygen–nitrogen–hydrogen analyzer (ONH-2000, Eltra, Haan, Germany) in a 99.995% pure He atmosphere. The other two were treated for X-ray diffraction (XRD) (D8 Advance, Bruker, Billerica, MA, USA) analysis and metalloscopic observations (BX51, Olympus, Tokyo, Japan).

Based on the alloying elements present in the samples obtained from the induction furnace and dried steel scrap, which was determined by employing the spark direct reading spectrometer, the recovery efficiencies of these elements in the alloy steel were calculated using Equation (1).

$$E_i = (mc)/(m_0c_0), \quad (1)$$

where E_i is the recovery efficiency of element i, m_0 is the amount of steel scrap added, c_0 is the content of element i in the steel scrap, m is the mass of the ingot, and c is the content of element i in the ingot.

3. Results

3.1. Recovery Percentages of Alloying Elements

The recovery efficiencies of the alloying elements (i.e., W, Cr, Ni, Mo, and V) in the induction furnace smelting process are shown in Table 3, which indicates that the average recovery efficiencies of all alloying elements were greater than 89.5 %, in the order Ni > W > Mo > Cr > V. The recovery efficiencies of Ni and W were stable with slight fluctuations, whereas that of V varied to a greater extent. This can be attributed to the reducibility and contents of the alloying elements and the operating conditions.

Table 3. Recovery percentages of alloying elements in smelting process (%).

No.	Steel Grade	W	Cr	Ni	Mo	V
1	H13-1	98.72	98.23	98.51	96.54	92.93
2	H13-2	98.46	93.85	98.76	98.50	94.90
3	H13-3	94.15	89.75	98.82	97.96	86.69
4	H13 + Ni	97.98	94.03	95.10	97.49	94.93
5	H13 + 2Mo	98.56	91.27	98.43	97.49	82.40
6	H13 + Ni + W	98.87	98.35	98.72	90.29	84.85
7	H13 + 2Ni + W	94.77	96.88	95.03	87.40	89.74
Average		97.36	94.62	97.63	95.09	89.49
Standard deviation		1.86	3.12	1.63	4.06	5.29

The contents of the alloying elements in the ingots obtained from the induction furnace steel are listed in Table 4. It is generally believed that the alloys show negligible losses during electroslag remelting.

Table 4. Contents of alloying elements in the ingots (wt%).

No.	Steel Grade	W	Cr	Ni	Mo	V	C	Si	Mn
1	H13-1	0.08	5.17	0.16	1.20	0.83	0.38	0.93	0.34
2	H13-2	0.07	5.08	0.20	1.17	0.80	0.41	0.86	0.31
3	H13-3	0.09	5.32	0.20	1.20	0.82	0.43	0.91	0.40
4	H13 + Ni	0.15	5.01	0.48	1.27	0.87	0.35	0.97	0.37
5	H13 + 2Mo	0.15	5.09	0.17	1.96	0.86	0.40	1.02	0.38
6	H13 + Ni + W	1.09	5.07	1.01	1.21	0.81	0.36	0.89	0.39
7	H13 + 2Ni + W	1.14	4.99	2.00	1.24	0.86	0.39	0.95	0.36

3.2. Impurity Element Content

The amounts of P and S in the steel scrap and samples are listed in Table 5. P and S concentrations in the samples are less than 0.02% and 0.006%, meaning a slight decrease than prior to smelting, which induction furnace melting can ensure for P and S contents.

Table 5. P and S contents in the steel scrap and the ingots from induction furnace (wt%).

		H13	H13 + Ni	H13 + 2Mo	H13 + Ni + W	H13 + 2Ni + W
P	Scrap	0.0199	0.0170	0.0170	0.0182	0.0197
	Sample	0.0169	0.0165	0.0165	0.0176	0.0174
S	Scrap	0.0056	0.0057	0.0050	0.0059	0.0046
	Sample	0.0053	0.0051	0.0039	0.0054	0.0040

For non-pretreatment steel scrap, after melting, hydrogen and oxygen contents in the samples are more than 3 ppm and 100 ppm, respectively. For the steel scrap with pretreatment of drying for 3–4 h, hydrogen and oxygen contents in the steel are less than 2 ppm and 25 ppm, and the nitrogen in molten steel is less than 60 ppm, as shown in Table 6, which indicates that drying steel scrap can inhibit the increase in impurity content.

Table 6. H, N, and O contents of steel scrap and the samples (ppm).

		H13	H13 + Ni	H13 + 2Mo	H13 + Ni + W	H13 + 2Ni + W
H	Scrap	1.8	1.5	1.5	1.7	1.6
	Sample	1.6	1.4	1.5	1.5	1.5
N	Scrap	55	56	54	55	53
	Sample	53	52	51	51	49
O	Scrap	18	25	21	25	24
	Sample	16	21	19	21	23

4. Discussion

4.1. Alloy Oxidation

During the heating process, Fe and the alloying elements are gradually oxidized within the molten steel owing to the acceleration of the mass transfer, which is different from the oxidation process before melting that takes place on the surface of the steel scrap. The oxidation reactions of W, Ni, Mo, Cr, V, and Fe in the molten steel are shown in Equations (2) to (7). In addition, the corresponding expressions of the standard Gibbs free energies of oxidation (ΔG^0) are listed (where T is the temperature (K); The ΔG^0 values of Ni, W, Mo, Cr, and V are based on the standard state of 1 mass% with Henry's law as reference). According to Ellingham diagram [41], the priority order of the alloying element oxidation is V, Cr, Mo, W and Ni; and with increasing temperature, the standard Gibbs free energies of oxidation increase.

$$[O] + [Ni] \rightarrow NiO \quad \Delta G^0 = -88,495 + 112.6T \ \text{J/mol} \tag{2}$$

$$[O] + 1/3[W] \rightarrow 1/3WO_3 \quad \Delta G^0 = -171,143 + 105.9T \ \text{J/mol} \tag{3}$$

$$[O] + 1/2[Mo] \rightarrow 1/2MoO_2 \quad \Delta G^0 = -185,755 + 112.3T \quad J/mol \tag{4}$$

$$[O] + 2/3[Cr] \rightarrow 1/3Cr_2O_3 \quad \Delta G^0 = -265,727 + 116.6T \quad J/mol \tag{5}$$

$$[O] + 2/3[V] \rightarrow 1/3V_2O_3 \quad \Delta G^0 = -270,010 + 112.5T \quad J/mol \tag{6}$$

$$[O] + Fe \rightarrow FeO \quad \Delta G^0 = -833,460 + 339.4T \quad J/mol \tag{7}$$

Considering that the oxidations proceed in a nonstandard state, it is necessary to discuss the reactions using Gibbs free energy. Here, taking Ni oxidation as an example, the expression of Gibbs free energy is presented in Equation (8). As shown, in addition to standard Gibbs free energy (ΔG^0), the activities of oxygen, alloying element and oxide (see second term on the right-hand side of Equation (8)) also exert effects on oxidations of alloying elements. Therefore the effects of the activities will be discussed in detail below.

$$\Delta G = \Delta G^0 + RT \ln\left(a_{(NiO)}/a_{[Ni]}a_{[O]}\right) \tag{8}$$

The effect of the activity of the oxygen in molten steel on the Gibbs free energy (ΔG) of each oxidation reaction is shown in Figure 2. As oxygen activity increases, ΔG decreases linearly. In the range of oxygen activity from 10^{-5} to 1, Gibbs free energies of Ni, W and Mo oxidation are much greater than zero, indicating that they have strong oxidation resistance. The ΔG values of V and Cr have their negative to positive transition points of oxygen activities, which correspond to the values of 0.05 and 0.02, respectively. These results indicate that oxygen concentration dramatically enhances the oxidation of V and Cr. Therefore, heating rapidly and reducing the air suction may alleviate the oxidation of the alloying elements. Additionally, Fe is the main constituent of alloy steel scrap; hence, according to the metallurgical principle, Fe is likely to oxidize first, forming FeO, which promotes the oxidization of the other alloying elements.

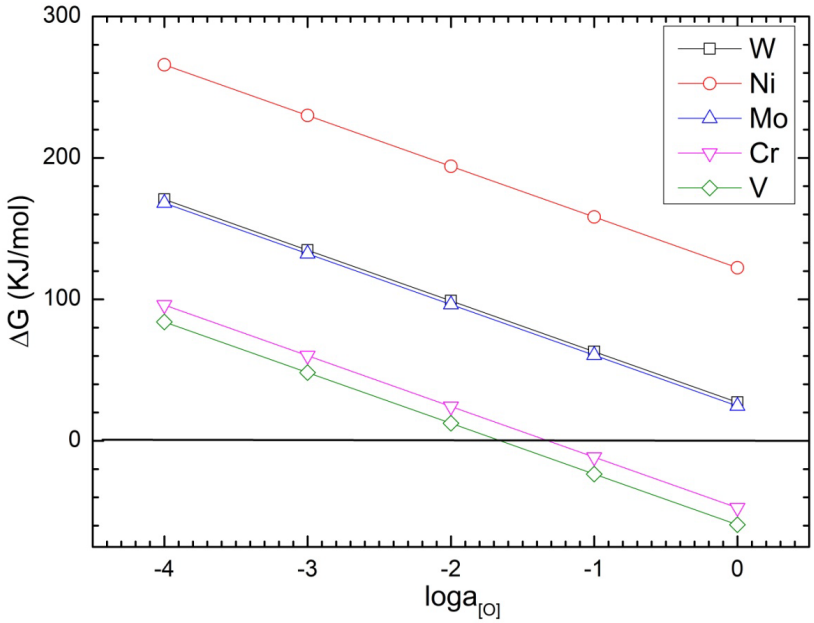


Figure 2. Effect of oxygen activity on the Gibbs free energy of oxidation for Ni, W, Mo, V and Cr at 1873 K.

The activity of the alloying element involves its concentration and activity coefficient, as shown in Equation (9). The activity coefficient in Equation (9) is obtained using

Equation (10) (only first-order interaction coefficients have been considered) that involves the interaction coefficients of different elements in steel.

$$a_i = f_i w_{[i]}, \tag{9}$$

$$\log f_i = \Sigma e_i^j [j\%], \tag{10}$$

where a_i is the activity of element i in the molten steel, f_i is the activity coefficient of element i in the molten steel, $w_{[i]}$ is the content of element i in the molten steel, e_i^j is the action coefficient of element j that is being exerted on element i, and $[j\%]$ is the content of element j in the molten steel.

Among the elements in the steel scrap (except for iron), the absolute interaction coefficient values of carbon element exerting on alloying elements are one or two orders of magnitude greater than that of S, P, Si and alloying elements, and has similar order of magnitude as that of O, N and H. Compared to the carbon, O, N and H in steel has a much lower concentrate. Therefore, among the elements, carbon plays a central role in influencing the activities of alloying elements. Figure 3 displays the effect of carbon on activity coefficients of Mo, Cr, and W at 1873 K. With increasing carbon content in molten steel, the activity coefficients of Mo, Cr, and W gradually decrease, whereas that of V significantly decreases. In contrast, Ni slightly increases, indicating that carbon effectively protects Mo, Cr, W, and V from oxidation, while enhancing the oxidation of Ni.

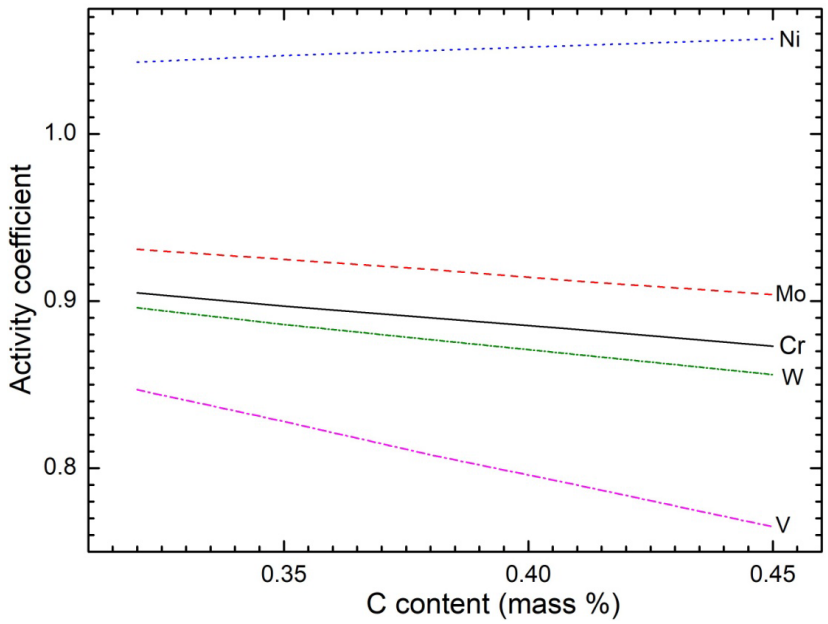


Figure 3. Effect of C content on activity coefficients of alloying elements at 1873 K.

Figure 4 shows ΔG of Ni, W, Mo, Cr, and V as a function of the concentration of the respective elements in the molten steel at a temperature of 1873 K with oxygen activity of 0.05. For the concentration range of 0.1 to 6.0, Gibbs free energies of Ni, W and Mo is significantly greater than zero, whereas that of V and Cr becomes negative at about 0.5 and 1.0 concentrations, respectively. These results indicate that, in liquid steel, higher contents (6%) of Ni, W and Mo show stronger ability to resist oxidation; whereas lower concentration (0.5%) of V is easily oxidized.

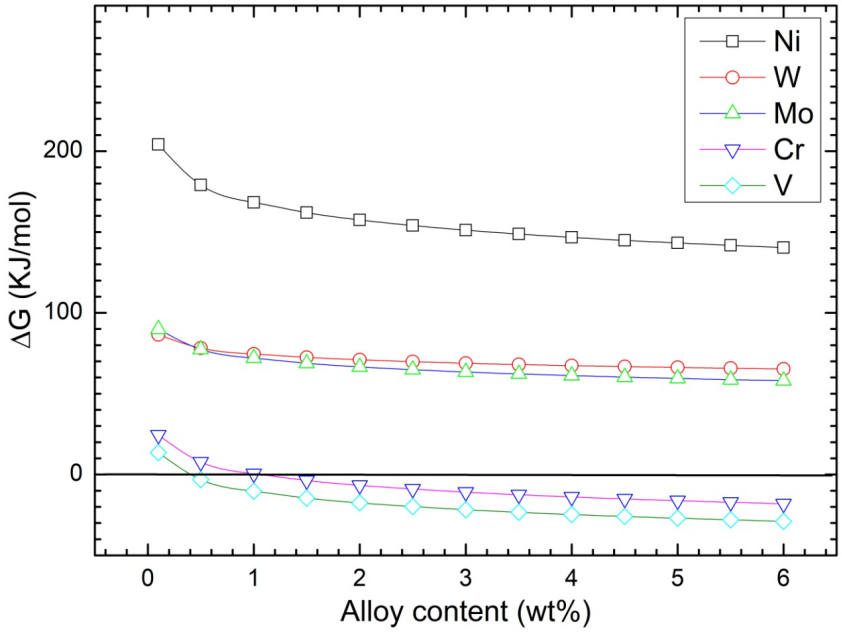


Figure 4. Effect of alloy concentration on the Gibbs free energy of oxidation at 1873 K.

The activity of oxide is particularly associated with its presence status. The SEM images of nonmetallic substance in the steel are shown in Figure 5, and their chemical compositions are listed in Table 7. In Figure 5a, it mainly comprises the oxides of Fe, V, and Cr, which could be the composite spinel of $(Fe,V,Cr)_3O_4$ [42,43]. As observed in Figure 5b, except for the above substances, it contains C, Si, and S, indicating a complex system. The formation of the spinel and complex system decreases the activities of FeO, V_2O_3, and Cr_2O_3, promoting the oxidation reactions of Fe, V, and Cr.

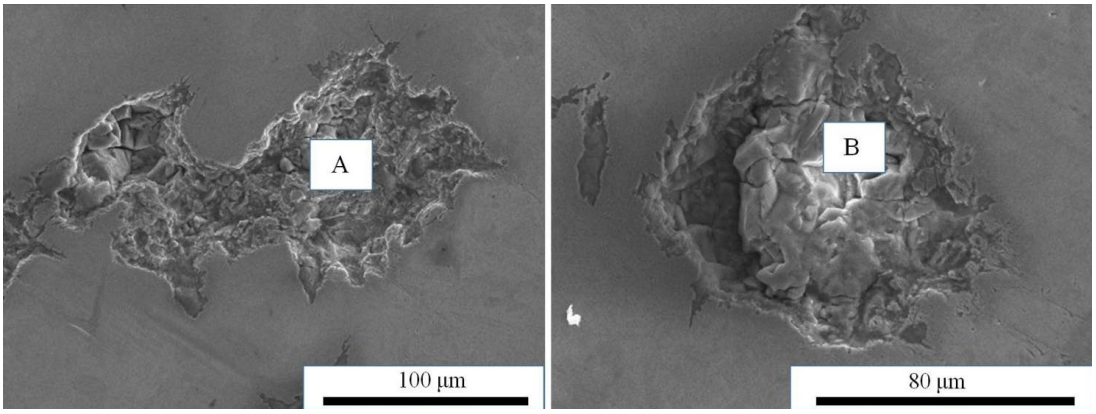


Figure 5. SEM images of the ingots from induction furnace ((**A**): spinel, (**B**): complex structure).

Table 7. Element contents in nonmetallic substance (EDS, atom%).

Element	O K	V K	Cr K	Fe K	C K	Si K	S K
A	52.15	4.97	15.52	27.36			
B	48.35	2.81	8.31	13.6	23.13	1.82	1.97

Among the factors, the oxygen content is a key factor for alloy oxidation. The fluctuation of the recovery efficiencies in Table 4 possibly derived from the intake of air or steam during the smelting process. Therefore, the introduction of air on the feedstock and during

smelting should be minimized. Using slag to cover the melt, as used herein, helps reduce the air intake.

4.2. Impurity Content Control

Generally, the phosphorus in molten steel is removed through oxidation based on its chemical property. Induction melting and electroslag remelting were conducted under non-oxidizing condition. Thus phosphorus contents in the samples had slight change before and after smelting. As for sulfur, the reducing slag used in the induction furnace and electroslag furnace have the compacity of desulfurization. However, sulfur content remains at a relatively low level in the steel scrap, and it cannot be further reduced considerably in the process.

Partial pressure of the nitrogen in air corresponds to equilibrium concentration of about 400 ppm in molten steel at 1873 K according to calculated result, which is much greater than nitrogen content in the steel scrap. Thus air suction may dramatically increase nitrogen content in molten steel. Air isolation using slag cover is one of the key measures to decrease nitrogen content.

The increase in hydrogen concentration may be attributed to the water attached to steel scrap. The reaction of hydrogen entering molten steel is shown in Equation (11). Figure 6 presents steam partial pressure influencing hydrogen concentration. With steam partial pressure increasing, hydrogen concentration increases exponentially, and a steam partial pressure of less than 10^{-4} ensures hydrogen concentration of less than two ppm in steel. Thus drying can reduce hydrogen content in the steel.

$$H_2O_{(gas)} = [O] + 2[H] \quad \Delta G^0 = 203,310 + 2.19T \text{ J/mol} \tag{11}$$

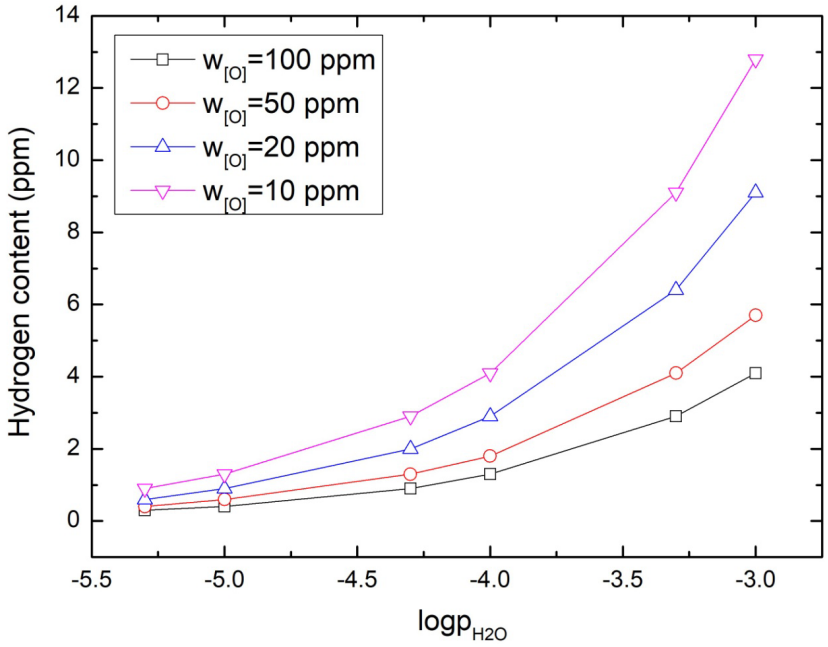


Figure 6. The effect of partial pressure of steam on hydrogen content in steel at 1873 K.

As shown in Equation (11), steam may result in an increase in oxygen content also. Furthermore, air suction plays an important role in the increase in oxygen content owing to high oxygen partial pressure in air.

In sum, reducing air suction can decrease oxygen and nitrogen contents, and drying steel scrap may reduce oxygen and hydrogen contents. In addition, after melting completely, argon injection decreases hydrogen, nitrogen and oxygen contents. For oxygen, the argon injection process removes the inclusions from molten steel in the induction furnace,

reducing the total oxygen content. Moreover, inclusions can be further removed in electroslag remelting process. Table 8 lists the number of inclusions in the electroslag ingots, with 90% of the inclusions having diameters smaller than 10 μm. The maximum diameter of the inclusions is smaller than 22 μm, and the inclusions are uniformly distributed in the ingots.

Table 8. Number and size of the inclusions in electroslag ingots (area: 1.5 × 1.5 cm).

Steel Grade	Size Range (μm)					Maximum Diameter
	<4	4–6	6–8	8–10	>10	
H13	9	18	15	7	3	19
H13 + Ni	21	19	10	4	6	21
H13 + Mo	13	14	11	10	5	16
H13 + W	61	21	7	2	3	17

4.3. Comparison of Smelting Methods

In the process of electric arc furnace smelting, the energy is concentrated in arc zone, and the temperature of the zone exceeds 3000 °C. For smelting carbon steel and low alloy steel scraps, electric arc furnace has greater flexibility than other steel-making furnaces, and can effectively remove impurities. However, for smelting medium and high alloy steel scraps, excessive temperature accelerates the oxidation of the alloys in the steel scrap, which results in massive losses of the alloys. In comparison, in the process of medium-frequency induction smelting, steel scrap is heated evenly, and excessive temperature zone can be avoided, attaining high recovery percent of the alloys.

According to production practice, the energy consumptions of the two smelting processes were approximately 1000 kWh per ton (electric arc furnace) and 700 kWh per ton (induction furnace), respectively. In addition, liquid steel from the electric arc furnace undergoes the ladle and RH refining processes. To ensure the quality of the high-performance steel, the ingots from the smelting process using electroslag remelting technology. The difference between the two methods is in the smelting stage. Notably, induction furnace smelting has certain advantages in terms of energy consumption.

Generally, differences in the processes lead to differences in the microstructures of steel. The ingots will be processed into final products through subsequent treatment, such as annealing, forging, and quenching. The microstructure of the ingot changes significantly during subsequent treatment, thereby influencing the properties of the steel. Thus, we will study the microstructure evolution in future.

5. Conclusions

Medium-frequency induction melting and electroslag remelting were conducted to treat medium and high alloy steel scrap to enhance the recovery percentages of the alloying elements and alleviate pollution. Based on the experimental and thermodynamic analysis results, the following conclusions can be drawn.

(1) In medium-frequency induction furnace melting, the average loss percentages of Ni, W, Mo, Cr, and V are 2.37%, 2.64%, 4.91%, 5.38%, and 10.51%, respectively. During smelting, the oxides of V and Cr may form spinels and a complex system, which can aggravate the recovery of the alloys.

(2) In the ingots, the content of P, S, N, H, and O slightly decreases compared to that in the original steel scrap, approximating 0.017%, 0.005%, 1.6, 50 and 21 ppm.

(3) The thermodynamic analysis results show that increasing the temperature increases the Gibbs free energies of the oxidation reactions; the decrease in the oxygen content significantly reduces the oxidation of the alloyed elements; with the increasing contents of the alloying elements, for V and Cr, the Gibbs free energies of oxidations change from positive to negative at 0.5 and 1.0 concentrations under an oxygen activity of 0.05; whereas, that of Ni, W and Mo remain positive in the concentration

range. Moreover, the spinel and complex system formation reduces the activity of oxide, which improves the oxidation of V and Cr.

(4) Compared to the electric arc furnace, medium-frequency induction melting attains a higher recovery percent of the alloys, and lower energy consumption.

The thermodynamic analysis and experimental results provide theoretical and practical directions for efficiently recycling the alloys in medium and high alloy steel scrap.

Author Contributions: Conceptualization, L.W. and Y.Z.; methodology, L.W.; software, K.L.; validation, H.M., K.L. and G.B.; formal analysis, Y.Z.; investigation, L.W.; resources, Y.Z.; data curation, H.M.; writing—original draft preparation, L.W.; writing—review and editing, Y.Z.; visualization, K.L.; supervision, H.W.; project administration, H.W.; funding acquisition, L.W. All authors have read and agreed to the published version of the manuscript.

Funding: This research was funded by the National Natural Science Foundation of China, grant number 51774001.

Data Availability Statement: Not applicable.

Conflicts of Interest: The authors declare no conflict of interest.

References

1. Hettich, D.; Aha, B.; Zimmermann, R.; Veldhuis, M.; Filzek, J. Lubricant—Reducing rcrap rates in forming high-alloyed steel by stable friction behavior over the temperature. *Procedia Manuf.* **2020**, *47*, 561–565. [CrossRef]
2. Zhang, L.; Su, S.P.; Liu, B.B.; Han, G.H.; Huang, Y.F.; Wang, Y.B.; Wang, Y.Z. Sustainable and high-efficiency recycling of valuable metals from oily honing ferroalloy scrap via de-oiling and smelting separation. *J. Hazard. Mater.* **2021**, *413*, e125399. [CrossRef] [PubMed]
3. Ohno, H.; Matsubae, K.; Nakajima, K.; Kondo, Y.; Nakamura, S.; Nagasaka, T. Toward the efficient recycling of alloying elements from end of life vehicle steel scrap. *Resour. Conserv. Recycl.* **2015**, *100*, 11–20. [CrossRef]
4. Ohno, H.; Matsubae, K.; Nakajima, K.; Nakamura, S.; Nagasaka, T. Development of Efficient Recycling System for Steel Alloying Elements in End of Life Vehicles. In *REWAS 2013*; Springer: Cham, Switzerland, 2013; pp. 414–422.
5. Xuan, Y.N.; Yue, Q. Scenario analysis on resource and environmental benefits of imported steel scrap for China's steel industry. *Resour. Conserv. Recycl.* **2017**, *120*, 186–198. [CrossRef]
6. Porzio, G.F.; Colla, V.; Fornai, B.; Vannucci, M.; Larsson, M.; Stripple, H. Process integration analysis and some economic-environmental implications for an innovative environmentally friendly recovery and pre-treatment of steel scrap. *Appl. Energy* **2016**, *161*, 656–672. [CrossRef]
7. Nechifor, V.; Calzadilla, A.; Bleischwitz, R.; Winning, M.; Tian, X.; Usubiaga, A. Steel in a circular economy: Global implications of a green shift in China. *World Dev.* **2020**, *127*, e104775. [CrossRef]
8. Yellishetty, M.; Mudd, G.M.; Ranjith, P.G.; Tharumarajah, A. Environmental life-cycle comparisons of steel production and recycling: Sustainability issues, problems and prospects. *Environ. Sci. Policy* **2011**, *14*, 650–663. [CrossRef]
9. Wübbeke, J.; Heroth, T. Challenges and political solutions for steel recycling in China. *Resour. Conserv. Recycl.* **2014**, *87*, 1–7. [CrossRef]
10. Golubev, O.V.; Korotchenko, A.S.; Chernousov, P.I. Predictions of scenarios for the consumption of scrap metal in ferrous metallurgy. *Metallurgist* **2011**, *54*, 649–655. [CrossRef]
11. Gao, M.; Gao, J.T.; Zhang, Y.L.; Yang, S.F. Simulation on scrap melting behavior and carbon diffusion under natural convection. *Int. J. Miner. Metall. Mater.* **2021**, *28*, 380–389. [CrossRef]
12. Li, J.H.; Provatas, N. Kinetics of scrap melting in liquid steel: Multipiece scrap melting. *Metall. Mater. Trans. B* **2008**, *39B*, 268–279. [CrossRef]
13. Diener, D.L.; Tillman, A.M. Scrapping steel components for recycling—Isn't that good enough? Seeking improvements in automotive component end-of-life. *Resour. Conserv. Recycl.* **2016**, *110*, 48–60. [CrossRef]
14. Ernst, C.; Wewers, B. Influence of residuals resulting from scrap use in the electric arc furnace process on the properties of hot-work tool steels. *J. Mater. Sci.* **2004**, *39*, 637–640. [CrossRef]
15. Kara, L.; Küçükömeroğlu, T.; Baran, O.; Efeoğlu, I.; Yamamoto, K. Microstructure, mechanical, and scratch resistance properties of TiAlCrNbN-graded composite coating deposited on AISI H13 steel substrate with pulsed DC closed field unbalanced magnetron sputtering method. *Metall. Mater. Trans. A* **2014**, *45*, 2123–2131. [CrossRef]
16. Varvara, D.A.I.; Tintelecan, M.; Aciu, C.; Boca, I.M.S.; Hădărean, A.; Rus, T.; Mare, R. An assessment of the substance losses from charge composition used to the steelmaking—Key factor for sustainable steel manufacturing. *Procedia Manuf.* **2019**, *32*, 15–21. [CrossRef]
17. Hou, Y.J.; Tian, H.M.; Qu, X.D.; Teng, J.Z.; Liu, G.X.; Li, Y. Development of digital control system for medium frequency induction furnaces. *IOP Conf. Ser. Earth Environ. Sci.* **2018**, *188*, 012005. [CrossRef]

18. Pan, H.T.; Lv, M. Analysis on the steelmaking characteristics of medium frequency induction furnace. *Ind. Heat.* **2015**, *55*, 18–23. (In Chinese)
19. Fleming, T.J.; Kavanagh, A.; Duggan, G.; O'Mahony, B.; Higgens, M. The effect of induction heating power on the microstructural and physical properties of investment cast ASTM-F75 CoCrMo alloy. *J. Mater. Res. Technol.* **2019**, *8*, 4417–4424. [CrossRef]
20. Megahed, H.; El-Kashif, E.; Shash, A.Y.; Essam, M.A. Effect of holding time, thickness and heat treatment on microstructure and mechanical properties of compacted graphite cast iron. *J. Mater. Res. Technol.* **2019**, *8*, 1188–1196. [CrossRef]
21. Zhang, P.; Li, Y.P.; Lei, Q.; Tan, H.; Shi, R.K.; She, J.L.; Li, S.Y.; Zhu, J.L.; Sheng, X.F.; Zhang, J.; et al. Microstructure and mechanical properties of a CuNiTi alloy with a large product of strength and elongation. *J. Mater. Res. Technol.* **2020**, *9*, 2299–2307. [CrossRef]
22. Liu, Y.; Wang, X.J.; Li, G.Q.; Huang, X.C.; Wang, Q.; Li, B.K. Cleanliness improvement and microstructure refinement of ingot processed by vacuum electroslag remelting. *J. Mater. Res. Technol.* **2020**, *9*, 1619–1630. [CrossRef]
23. Jiang, Z.H.; Dong, Y.W.; Liang, L.K.; Li, Z.B. Hydrogen pick-up during electroslag remelting process. *J. Iron Steel Res. Int.* **2011**, *18*, 19–23. [CrossRef]
24. Wang, Q.; He, Z.; Li, G.G.; Li, B.K.; Zhu, C.Y.; Chen, P.J. Numerical investigation of desulfurization behavior in electroslag remelting process. *Int. J. Heat Mass Trans.* **2017**, *104*, 943–951. [CrossRef]
25. Wang, Q.; Li, G.Q.; He, Z.; Li, B.K. A three-phase comprehensive mathematical model of desulfurization in electroslag remelting process. *Appl. Therm. Eng.* **2017**, *114*, 874–886. [CrossRef]
26. Wang, Q.; Liu, Y.; Li, G.Q.; Gao, Y.M.; He, Z.; Li, B.K. Predicting transfer behavior of oxygen and sulfur in electroslag remelting process. *Appl. Therm. Eng.* **2018**, *129*, 378–388. [CrossRef]
27. Guo, Y.F.; Xia, Z.B.; Li, Q.; Sun, M.Y.; Liu, W.F.; Wang, S.G.; Shen, Z.; Zheng, T.X.; Ding, B.; Zhong, Y.B. Motion and removal behavior of inclusions in electrode tip during magnetically controlled electroslag remelting: X-ray microtomography characterization and modeling verification. *J. Mater. Sci. Technol.* **2022**, *96*, 1–10. [CrossRef]
28. Qiu, G.X.; Zhan, D.P.; Li, C.S.; Yang, Y.K.; Jiang, Z.H.; Zhang, H.S. Effects of electroslag remelting process and Y on the inclusions and mechanical properties of the CLAM steel. *Nucl. Eng. Technol.* **2020**, *52*, 811–818. [CrossRef]
29. Jagota, V.; Sharma, R.K. Impact of austenitizing temperature on the strength behavior and scratch resistance of AISI H13 steel. *J. Inst. Eng. India Ser. D* **2020**, *101*, 93–104. [CrossRef]
30. Abbasi, E.; Luo, Q.S.; Owens, D. Case study: Wear mechanisms of NiCrVMo-steel and CrB-steel scrap shear blades. *Wear* **2018**, *398–399*, 29–40. [CrossRef]
31. Alvim, A.C.; Ferreira, J.R.; Pereira, R. The enhanced normalized normal constraint approach to multi-objective robust optimization in helical milling process of AISI H13 hardened with crossed array. *Int. J. Adv. Manuf. Technol.* **2021**, *119*, 2763–2784. [CrossRef]
32. Suhaily, M.; Amin, A.N.; Patwari, M. Machinability Improvement by Workpiece Preheating during End Milling AISI H13 Hardened Steel. *Adv. Mater. Res.* **2011**, *264–265*, 888–893. [CrossRef]
33. Shi, Z.R.; Wang, R.Z.; Su, H.; Chai, F.; Wang, Q.F.; Yang, C.F. Effect of nitrogen content on the second phase particles in V–Ti microalloyed shipbuilding steel during weld thermal cycling. *Mater. Des.* **2016**, *96*, 241–250. [CrossRef]
34. Hosseini, V.A.; Wessman, S.; Hurtig, K.; Karlsson, L. Nitrogen loss and effects on microstructure in multipass TIG welding of a super duplex stainless steel. *Mater. Des.* **2016**, *98*, 88–97. [CrossRef]
35. Lee, S.J.; Jung, Y.S.; Baik, S.I.; Kim, Y.W.; Kang, M.; Woo, W.; Lee, Y.K. The effect of nitrogen on the stacking fault energy in Fe–15Mn–2Cr–0.6C–xN twinning-induced plasticity steels. *Scr. Mater.* **2014**, *92*, 23–26. [CrossRef]
36. Ye, Y.X.; Ouyang, B.; Liu, C.Z.; Duscher, G.J.; Nieh, T.G. Effect of interstitial oxygen and nitrogen on incipient plasticity of NbTiZrHf high-entropy alloys. *Acta Mater.* **2020**, *199*, 413–424. [CrossRef]
37. Allam, T.; Guo, X.F.; Chwałek, M.L.; Hamada, A.; Ahmed, E.; Bleck, W. Impact of precipitates on the hydrogen embrittlement behavior of a V-alloyed medium-manganese austenitic stainless steel. *J. Mater. Res. Technol.* **2020**, *9*, 13524–13538. [CrossRef]
38. Nunes, A.R.V.; Zeemann, A.; de Almeida, L.H. The contribution of impurities to unexpected cold cracks in a thick C-Mn steel plate. *J. Mater. Res. Technol.* **2019**, *8*, 4364–4373. [CrossRef]
39. Anijdan, S.H.M.; Arab, G.; Sabzi, M.; Sadeghi, M.; Eivani, A.R.; Jafarian, H.R. Sensitivity to hydrogen induced cracking, and corrosion performance of an API X65 pipeline steel in H_2S containing environment: Influence of heat treatment and its subsequent microstructural changes. *J. Mater. Res. Technol.* **2021**, *15*, 1–16. [CrossRef]
40. Cooper, A.J.; Cooper, N.I.; Dhers, J.; Sherry, A.H. Effect of oxygen content upon the microstructural and mechanical properties of type 316L austenitic stainless steel manufactured by hot isostatic pressing. *Metall. Mater. Trans. A* **2016**, *47*, 4467–4475. [CrossRef]
41. Hasegawa, M. Chapter 3.3—Ellingham Diagram. In *Treatise on Process Metallurgy*; Seetharaman, S., Ed.; Elsevier: Stockholm, Sweden, 2014; pp. 507–516.
42. Xie, W.; Xing, X.R.; Cao, Z.M. Thermodynamic assessment of the Fe–V–O system. *Calphad* **2020**, *71*, e102213. [CrossRef]
43. Liu, C.S.; Liu, X.Q.; Ni, H.W.; Yang, S.F.; Li, J.S.; Ye, F. Effect of vanadium on modification of inclusions in Mn- and Si-deoxidized steel during heat treatment at 1473 K. *J. Iron Steel Res. Int.* **2017**, *24*, 520–528. [CrossRef]